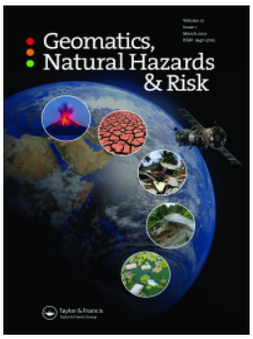

Geomatics, Natural Hazards and Risk

ISSN: 1947-5705 (Print) 1947-5713 (Online) Journal homepage: www.tandfonline.com/journals/tgnh20

Earthquake induced liquefaction hazard analysis for Chittagong City using machine learning

Md. Mehedi Hasan, Md. Zillur Rahman & Abul Kashem Faruki Fahim

To cite this article: Md. Mehedi Hasan, Md. Zillur Rahman & Abul Kashem Faruki Fahim (2025) Earthquake induced liquefaction hazard analysis for Chittagong City using machine learning, Geomatics, Natural Hazards and Risk, 16:1, 2451126, DOI: 10.1080/19475705.2025.2451126

To link to this article: https://doi.org/10.1080/19475705.2025.2451126

Published online: 19 Jan 2025.

GEOMATICS, NATURAL HAZARDS AND RISK
2025, VOL. 16, NO. 1, 2451126
https://doi.org/10.1080/19475705.2025.2451126

Taylor & Francis
Taylor & Francis Group

Earthquake induced liquefaction hazard analysis for Chittagong City using machine learning

Md. Mehedi Hasan, Md. Zillur Rahman and Abul Kashem Faruki Fahim

Department of Disaster Science and Climate Resilience, University of Dhaka, Dhaka

ABSTRACT

Liquefaction hazard analysis is crucial in earthquake-prone regions as it magnifies structural damage. In this study, standard penetration test (SPT) and shear wave velocity (V_s) data of Chittagong City have been used to assess the liquefaction resistance of soils using artificial neural network (ANN). For a scenario of 7.5 magnitude (Mw) earthquake in Chittagong City, estimating the liquefaction-resistance involves utilizing peak horizontal ground acceleration (PGA) values of 0.15 and 0.28 g. Then, liquefaction potential index (LPI) is determined to assess the severity of liquefaction. In most boreholes, the LPI values are generally higher, with slightly elevated values in SPT data compared to V_s data. The current study suggests that the Valley Alluvium, Beach and Dune Sand may experience extreme liquefaction with LPI values ranges from 9.55 to 55.03 and 0 to 37.17 for SPT and V_s respectively, under a PGA of 0.15 g. Furthermore, LPI values ranges from 25.55 to 71.45 and 9.55 to 54.39 for SPT and V_s correspondingly. The liquefaction hazard map can be utilized to protect public safety, infrastructure, and to create a more resilient Chittagong City.

ARTICLE HISTORY
Received 12 September 2024
Accepted 5 January 2025

KEYWORDS
Liquefaction potential index (LPI); factor of safety (FS); artificial neural network (ANN); limit state function (LSF); surface geology; Chittagong City

1. Introduction

Liquefaction hazard analysis is a critical aspect of assessing seismic risk in areas prone to earthquakes. Chittagong City, Bangladesh, is particularly vulnerable to seismic events due to its geographical location near active tectonic plate boundaries. Earthquake-induced liquefaction poses a significant threat to regions with loose sediments and seismic activity (Rahman and Siddiqua 2017). Liquefaction is the change of granular soil from a solid to a liquefied condition as a result of increased pore water pressure and decreased effective stress following an earthquake (Marcuson 1979). During an earthquake, soil liquefaction can amplify the damage caused by seismic shaking which was demonstrated by Alaska and Niigata earthquake in 1964, the 1999 Chi-Chi earthquake and the earthquake in Sulawesi in 2018 (Ku et al. 2004;

CONTACT Md. Zillur Rahman zillur@du.ac.bd

Sassa and Takagawa 2019; Seed and Idriss 1967; Youd and Idriss 2001). Therefore, when water-saturated quaternary loose sediments are present within 20 meters of the surface, liquefaction hazard analysis is required in earthquake-prone regions in order to evaluate the seismic risk (Hossain et al. 2020).

Liquefaction resistance of soils can be assessed using the cyclic triaxial test, moreover, in-situ tests like the SPT measurement, Cone Penetration Test (CPT), and V_s measurement. To conduct laboratory experiments for the assessment of liquefaction-resistance, undisturbed soil samples of superior quality are required. However, it can occasionally be challenging and expensive to gather undisturbed samples were taken from muddy, loose, sandy, and waterlogged soils. As a result, *in situ* tests are preferable for analyzing soil liquefaction which is convenient and affordable (Seed et al. 1983; Seed and Idriss 1971). Over the past five decades, liquefaction potential analysis has been conducted applying simplified process, which was first proposed by Seed and Idriss (1971). Since it was first developed in 1971, numerous researchers have adjusted, calibrated, and updated this process (Juang et al. 2000, 2002, 2003; Robertson et al. 1992; Robertson and Wride 1998). Corrected SPT are frequently utilized as an input in simplified processes (Seed et al. 1983; Youd and Idriss 2001).

Another popular method, for assessing liquefaction resistance is CPT where continuous penetration resistance profile is used for stratigraphic analysis (Robertson and Wride 1998; Youd and Idriss 2001). The primary benefit of this procedure is that CPT findings are typically more reliable, reproducible, and consistent (Robertson and Wride 1998; Youd and Idriss 2001). Soil liquefaction resistance is assessed using the corrected cone penetration test tip resistance through CPT.

The V_s method suggested by Andrus and Stokoe (2000) is a more practical and cost-effective alternative to the SPT for liquefaction assessment. When conducting SPT and CPT is challenging because of stiff soils or to extract undisturbed samples, V_s method can be conducted those places. Small strain shear modulus, which is necessary for calculating dynamic soil reaction and conducting soil structure interaction investigations, is directly connected to V_s (Robertson and Wride 1998).

The loose and soft Quaternary sediments cover over 80% of Bangladesh's land area (Hossain et al. 2020). Large-scale liquefaction phenomena were seen in Bangladesh's alluvial deposits following the Great Indian Earthquake in 1897, the Bengal Earthquake of 1885, and the Srimangal Earthquake in 1918 (Hossain et al. 2020). In Habiganj, after the 1897 Great Indian Earthquake, several sand dikes have been discovered on the about 2-meter-high wall of a reservoir carved into the alluvial sediments as a result of liquefaction (Morino et al. 2014). Continuous plate boundary tectonic displacement and active faults, historical earthquake episodes warn us that Bangladesh is susceptible to earthquakes of a moderate to high magnitude (Rahman et al. 2015). When a destructive earthquake occurs in a developing like Bangladesh and underdeveloped country, it may cause a significant amount of lives, infrastructural damage and reverse their development (Bilham 2009). One of the main causes of the rise in infrastructure damage is the liquefaction of the soil. Hence, reliable liquefaction hazard analysis is crucial for ensuring the safety of densely populated areas like Chittagong City.

Rahman and Siddiqua (2017) used V_s and SPT to analyze the liquefaction resistance of Sylhet, Chittagong, and Dhaka. Rahman et al. (2015) applied cumulative frequency distribution and LPI, they quantitatively assessed liquefaction risk following the simplified procedure for Dhaka city. A probabilistic model for evaluating liquefaction potential using multi-gene genetic programming (MGGP) based on post-liquefaction SPT, CPT and V_s data developed by Muduli et al. (2014); Muduli and Das (2013, 2015a). They also compared its accuracy to ANN and statistical models and found a better result, although ANN had provided a satisfactory result. Muduli and Das (2014b) utilized SPT data to create liquefaction index model using MGGP, where ANN's liquefaction prediction accuracy was 86% whereas MGGP's prediction accuracy was just one percent higher. Muduli and Das (2015b, 2015c) created a liquefaction model based on SPT and CPT data using MGGP, incorporating reliability analysis. This model uses MGGP to calculate CRR, and uncertainty is estimated using a lognormal distribution and Bayesian analysis. Muduli and Das (2014a) proposed a MGGP-based model using CPT data for liquefaction assessment where they found 91% accuracy for the prediction of liquefaction occurrence from an ANN model. In the perspective of Bangladesh, Fahim et al. (2022) used ANNs to predict CRR directly from SPT and V_s data Dhaka City and found reliable results. These studies show that ANN can achieve satisfactory accuracy and offer an efficient, flexible approach to CRR and liquefaction potential estimation, making it a suitable choice for the current analysis.

This study proposes a novel approach using machine learning to enhance liquefaction hazard analysis in Chittagong City. A performance function developed by Seed and Idriss (1971) is called the limit state function (LSF), within a neural network framework according to Juang et al. (2002, 2003) to compute CRR that significantly overcomes the limitations of traditional methods and achieves greater accuracy in predicting liquefaction susceptibility.

The seismically active Chittagong-Myanmar fold and thrust belt (CMFB), runs through eastern Bangladesh which increases the earthquake susceptibility of Chittagong (Bürgi et al. 2021). According to the Bangladesh National Building Code (BNBC), Chittagong City has been delineated seismically in zone 3, where the peak ground acceleration is 0.28 g, which corresponds to a 2% chance of exceeding 50 years (a 2475-year return period). There are only a few literatures available about liquefaction hazard for Chittagong City, with limited SPT and V_s data. But there is no one using Machine Learning, while machine learning provides more precise results than the simplified procedure (Shahin et al. 2001). Hence, liquefaction hazard analysis is extremely important for this densely populated city to minimize casualties and property damage. As a result of the extreme variability in characteristics of the soil and seismic conditions, it is challenging to select a suitable regression analysis empirical equation using SPT, CPT, and V_s techniques (Xue and Liu 2017). Compared to traditional empirical and statistical methods, machine learning has the benefit that they do not necessitate a prior understanding of the mechanisms behind the relationship between the input/output variables while potentially offering greater accuracy (Shahin et al. 2001). Building upon previous research in Dhaka and Sylhet, the goal is to provide a comprehensive liquefaction hazard map for Chittagong City, contributing to effective mitigation strategies and safeguarding lives and infrastructure.

2. Surface geology of the study area

Chittagong is a large port city on the southeastern coast of Bangladesh. East of the India-Eurasia clash, there is an accretionary wedge with a northerly tendency called the seismically active CMFB, is where eastern Bangladesh is located. Southeast Bangladesh's Chittagong City is located at the estuary of the Karnaphuli River (Figure 1). According to the BNBC, Chittagong City falls under zone three, where PGA is 0.28 g which equivalent to two percent probability of exceedance in fifty years. Chittagong City was formed as a result of Holocene alluvial and coastal plains, as well as folded Tertiary sedimentary rocks (Rahman and Siddiqua 2017). Clay, silt, and loose sand make up the alluvial and coastal plains, whereas sandstone, siltstone, and shale, which are soft rocks, make up the Tertiary rocks (Rahman and Siddiqua 2017).

The Tertiary sedimentary hills in the city's center, which run from northwest to southeast, are made up of siltstone, shale, and soft sandstone. Shallow valleys with deposits of silt and sand are interspersed with worn and deteriorated shale and/or sandstones that overlay these rocks. The city's steep regions vary in elevation from 10 to 79 meters. Large amounts of sediments (sand, silt, and clay) from rivers, delta plains, and floodplains have collected in the alluvial and coastal plains of the hilly region's western, eastern, and southern regions as a result of the fine-grained sediments eroded off the hills. The elevation of the alluvial and coastal plains fluctuates between zero to ten meters. Fine-grained sediments are eroded from the hills in the western, eastern, and southern regions of the hilly area and are deposited on alluvial and coastal plains. These deposits build up to form thick sediments made of sand, silt, and clay in a variety of environments, including fluviatile, delta plain, and floodplain. The elevation of the alluvial and coastal plains ranges from 0 to 10 meters. Thus, it is imperative that this city do a liquefaction hazard analysis in order to increase resilience.

The present study generates the Chittagong City surface geology map using the engineering geological and geomorphological maps previously developed by CDMP (2009). Based on the environment, depositional history, lithology, and geomorphology, six surface geological units comprise the city (Figure 1) Three geological units also separate the city's subterranean materials which are Tertiary sedimentary rock (TR), Holocene clay-based soil (HC), and Holocene sand-based soil (HS) (Rahman and Siddiqua 2016). The sedimentary rocks of the Tertiary period consist of siltstone, shale, and soft sandstone. Subsurface materials found in 48 boreholes are categorized to a depth of thirty meters. Figure 2 illustrates the subsurface material classification found in Chittagong City boreholes.

3. Seismotectonics

South Asian nation of Bangladesh is prone to earthquakes in (Figure 3). Over the past 250 years, East Bengal and Northeast India have experienced numerous historical earthquakes (Table 1). The Great Indian Earthquakes of 1897, 1918 Srimangal, 1885 Bengal, and 1762 Bengal-Arakan were notable among them. These earthquakes had magnitudes of 7.5, 7.0, 7.6, and 8.7, in that order. Chittagong City sustained

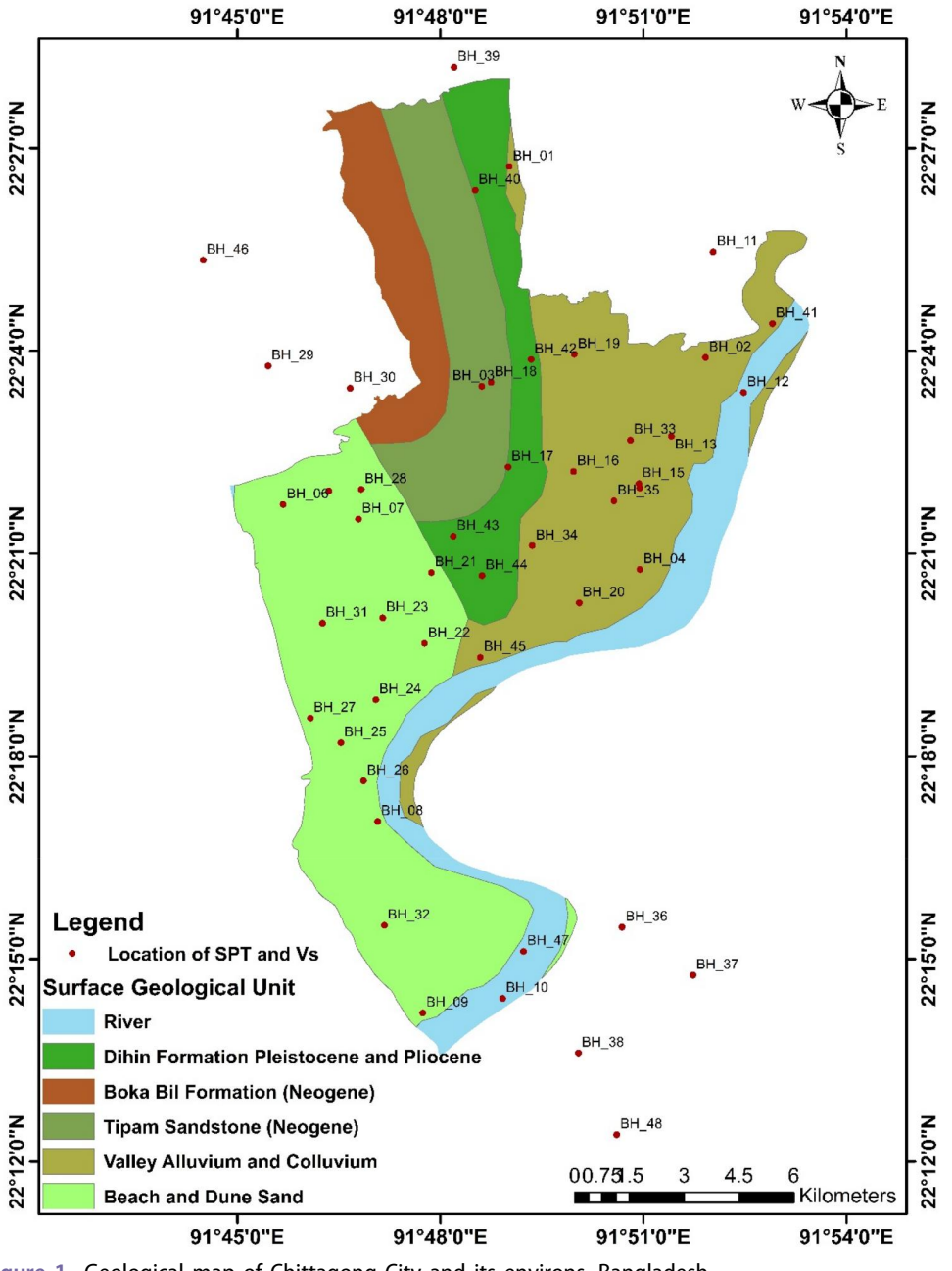

Figure 1. Geological map of Chittagong City and its environs, Bangladesh.

significant damage from the earthquake in Bengal-Arakan, which struck near to the city. In recent years, a number of earthquakes with magnitudes vary between 4.0 to 6.0 have happened near Chittagong City. The city was also slightly harmed by these earthquakes, as evidenced by the tilting and breaking of building walls.

In the center of the Bay of Bengal is the Bengal Basin, primarily made up of Bangladesh. Bangladesh and a portion of the nearby the Indian states of Assam,

Depth (m)	BH-1	BH-2	BH-3	BH-4	BH-5	BH-6	BH-7	BH-8	BH-9	BH-10	BH-11	BH-12	BH-13	BH-14	BH-15	BH-16	BH-17	BH-18	BH-19	BH-20	BH-21	BH-22	BH-23	BH-24	BH-25	BH-26	BH-27	BH-28	BH-29	BH-30	BH-31	BH-32	BH-33	BH-34	BH-35	BH-36	BH-37	BH-38	BH-39	BH-40	BH-41	BH-42	BH-43	BH-44	BH-45	BH-46	BH-47	BH-48
1.5	HC	HC	HC	HC	HC	HC	HC	HC	HS	HC	HS	HC	HC	HC	HC	HS	HC	HC	HC	HC	HC	HC	HC	HC	HS	HC	HS	HS	HC	HC	HC	HS	HS	HC	HC	HS	HC	HC	HC	HC	HS	HC	HC	HS	HC	HC	HS	HS
3.0	HC	HC	HC	HC	HC	HC	HC	HC	HS	HC	HS	HC	HC	HC	HC	HS	HC	HC	HC	HC	HS	HC	HC	HS	HS	HC	HS	HS	HC	HC	HC	HS	HS	HC	HC	HC	HS	HC	HC	HC	HC	HS	HC	HS	HC	HC	HS	HS
4.5	HC	HC	HC	HC	HC	HC	HS	HS	HC	HC	HS	HC	HC	HC	HC	HS	HC	HC	HC	HC	HS	HC	HC	HS	HS	HC	HS	HS	HC	HC	HC	HS	HS	HC	HC	HC	HS	HC	HC	HC	HC	HS	HC	HC	HC	HC	HS	HS
6.0	HC	HC	HC	HC	HC	HC	HS	HS	HC	HC	HS	HC	HC	HC	HC	HC	HC	HC	HC	HC	HS	HC	HC	HS	HS	HS	HS	HC	HC	HC	HS	HS	HC	HC	HC	HC	TR	HC	HC	HC	HC	HC	HS	HC	HS	HS	HS	HS
7.5	HC	HC	HC	HC	HC	HS	HS	HS	HC	HS	HC	HC	HC	HC	HC	HC	HC	HS	HC	HC	HS	HS	HS	HS	HS	HS	HS	HC	HC	HC	HC	HC	HC	HC	HC	HC	TR	HC	HC	HC	HC	HC	HC	HS	HC	HS	HS	HS
9.0	HC	HC	HC	HC	HS	HC	HC	HC	HC	HS	HS	HC	HC	HC	HC	HC	HC	HS	HC	HC	HS	HS	HS	HC	HC	HS	HS	TR	HC	HC	HC	HC	HC	HC	HC	HC	TR	HC	HC	HC	HC	HC	HC	HS	HS	HS	HS	HS
10.5	HC	HC	HC	HC	HC	HC	HC	HS	HS	HS	HS	HC	HC	HC	HS	HC	HC	HS	HC	HC	HS	HS	HS	HC	HC	HS	HS	TR	HC	HC	HC	HS	HS	HS	HC	HC	TR	TR	HC	HC	HC	HS	HC	TR	HS	HC	HS	HS
12.0	HC	HC	HC	HC	HC	HC	TR	HS	HS	HS	HS	HC	HC	HC	HS	HC	HC	HS	HS	HC	HC	HS	HS	HS	HS	HS	HS	TR	TR	HC	HS	HS	HS	HC	HC	TR	TR	HC	HC	HC	HS	HC	TR	TR	HC	HS	HS	TR
13.5	HC	HC	HC	HC	HC	HC	TR	HS	HS	HS	HS	HC	HC	HC	HS	HC	HC	TR	HS	HC	HC	HS	HS	HC	HC	HS	HS	HS	TR	TR	TR	HS	HS	HS	HS	HC	TR	TR	HC	HC	HC	HS	HC	TR	TR	HS	HS	TR
15.0	HC	HC	HC	HS	TR	HC	TR	HC	HS	HC	HS	HS	HS	HC	HS	HC	HC	HC	TR	HS	HC	HS	HS	HS	HS	HS	HS	HS	TR	TR	TR	HS	HS	HS	TR	HC	TR	TR	HS	HC	TR	HS	HS	TR	TR	HS	TR	TR
16.5	HC	HC	HC	HS	TR	HC	TR	HC	HS	HC	HS	HS	HC	HS	HS	HS	TR	TR	HS	HS	TR	HC	HS	HS	HS	HS	HC	TR	TR	TR	HS	HS	HS	TR	HS	TR	TR	HS	HC	TR	HS	HS	TR	TR	HS	TR	TR	TR
18.0	HC	HC	HC	HS	TR	HS	TR	HC	HC	TR	HC	HS	HS	HS	HC	HS	TR	TR	HS	HS	TR	HC	HS	HS	HC	HS	HC	TR	TR	TR	HS	HS	HS	TR	HS	TR	TR	HS	HC	TR	HS	HC	TR	TR	HS	TR	TR	TR
19.5	HC	HC	HS	HS	TR	HC	TR	HS	HS	TR	HC	HC	HS	HS	HC	TR	TR	TR	HC	HS	TR	HC	HC	HS	HC	HS	HC	TR	TR	TR	HS	HS	HS	TR	HS	TR	TR	HS	HC	TR	HS	HC	TR	TR	HS	TR	TR	TR
21.0	HC	HC	TR	HC	TR	HS	TR	HS	HS	TR	HC	HC	HC	HS	HC	TR	TR	TR	HS	TR	TR	HC	HC	HC	HC	HS	HC	TR	TR	TR	HS	HS	HS	TR	HS	TR	TR	TR	HC	TR	HS	HC	TR	TR	HC	TR	TR	TR
22.5	HC	HC	TR	HS	TR	TR	TR	HC	HS	TR	HC	HC	HC	HC	HC	TR	TR	TR	HS	TR	TR	HC	HC	HC	HC	HC	HC	TR	TR	TR	HS	HS	HS	TR	HS	TR	TR	TR	HC	TR	HS	HC	TR	TR	TR	TR	TR	TR
24.0	HS	HC	TR	HS	TR	TR	TR	HC	HS	TR	HC	HC	HC	HC	HC	TR	TR	TR	HS	TR	TR	HS	HC	HC	HC	HC	HC	TR	TR	TR	HS	HS	HS	TR	HS	TR	TR	TR	HC	TR	HS	HC	TR	TR	TR	TR	TR	TR
25.5	HS	HC	TR	HC	TR	TR	TR	HC	TR	TR	HC	HC	HC	HC	HC	TR	TR	TR	HC	TR	TR	HS	HC	HS	HC	HC	HC	HC	TR	TR	TR	HS	HS	TR	HS	TR	TR	TR	TR	HC	TR	HC	HC	TR	TR	TR	TR	TR
27.0	HC	HC	TR	HC	TR	TR	TR	HS	TR	TR	HC	HC	HC	HC	HS	TR	TR	TR	HC	TR	TR	HS	HC	HS	HC	HC	HC	HC	TR	TR	TR	HS	HS	TR	HS	TR	TR	TR	TR	HC	TR	HC	TR	TR	TR	TR	TR	TR
28.5	HC	HC	TR	HC	TR	TR	TR	HS	TR	TR	HC	HC	HC	HC	HS	TR	TR	TR	HC	TR	TR	HS	HC	HS	HC	HC	HC	HC	TR	TR	TR	HS	HS	TR	HS	TR	TR	TR	TR	HC	TR	HC	TR	TR	TR	TR	TR	TR
30.0	HC	HC	TR	HC	TR	TR	TR	HS	TR	TR	HC	HC	HC	HC	HS	TR	TR	TR	HC	TR	TR	HS	HC	HS	HC	HC	HC	HC	TR	TR	TR	HS	HS	TR	HS	TR	TR	TR	TR	HC	TR	HC	TR	TR	TR	TR	TR	TR

Figure 2. The subsurface materials' categorization found in 48 Chittagong City boreholes. Holocene clay-based soil, Holocene sand-based soil, and sedimentary rock in Tertiary phase (shale, siltstone and soft sandstone) are denoted by the letters HC, HS, and TR, respectively (Rahman and Siddiqua 2016).

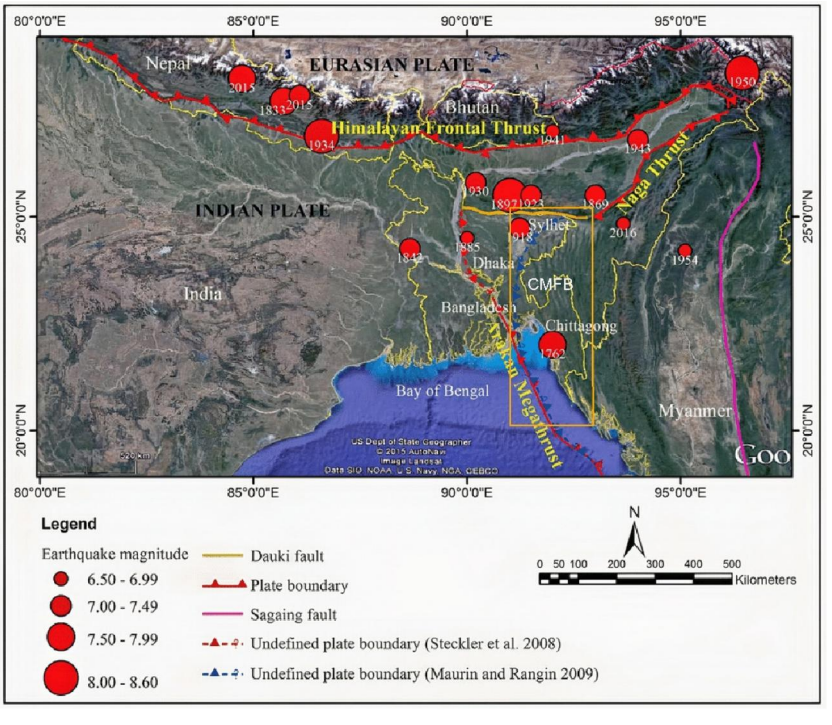

Figure 3. Historical and recent earthquakes greater than Mw 6.5 which have took place from 1762 to 2016 (modified from Rahman and Siddiqua (2017)).

Tripura, and West Bengal are included in the vast region of the northeastern Indian Plate that is known as the Bengal Basin. Bangladesh occupies almost three-quarters of the Bengal Basin. The Bengal Basin is bordered by the southern Bay of Bengal, the

Table 1. Significant earthquakes that have damaged and killed people in Bangladesh over the past 256 years (Rahman et al. 2020).

Date	The earthquake's name	Moment Magnitude (Mw)	Quantity of fatalities	Damage to structures
2nd April, 1762	Bengal-Arakan Earthquake	8.5	500 in Dhaka	Dhaka and Chittagong had a pretty severe earthquake.
14 July, 1885	Bengal Earthquake	6.87	Not revealed	The areas with the greatest damage were Mymensingh, Sirajganj, Jamalpur, and Bogura. Considering other regions situated at a comparable length from the focal point, the damage in Dhaka was relatively minimal.
12 June, 1897	Great Assam Earthquake	8.03	545 in Sylhet	Shillong, Assam, India, reported the most damage. Nearly every masonry structure in Dhaka had significant damage, with some completely collapsing. The majority of the masonry structures in Sylhet suffered significant damage.
8th July, 1918	Srimangal Earthquake	7.10	No precise figures were disclosed	In Srimangal (Moulvibazar), the majority of the tea mills and bungalows were harmed. There were reports of major damage in Agartala, Sylhet, Habiganj, and Kishoreganj, India. A few of the buildings in Dhaka had minor cracks.

Arakan Yoma Folded Belt System in the east, the Precambrian northern Shilling Massif, and the Indian Platform in the west (Rahman and Siddiqua 2016). The study area is located in Bangladesh's western Eastern Folded Belt region in (Figure 3). The yellow rectangle of Figure 3 shows the CMFB.

The majority of the western Indian subcontinent's significant historical earthquakes have occurred in areas that cross the plate border where it connects to both plates (Figure 3).

According to Bilham and Hough (2006), the Indian Plate is shifting 4 cm per year toward the north and 6 cm per year toward the northeast. The velocity at which the plate moves ahead (rate of convergence) and the high frequency of massive earthquakes recorded nearby have led to the classification of the northern and northeastern regions of India, which include Bangladesh, Nepal, and Bhutan, as seismic zones. Magnitudes ranging from M 7.5 to M 8.5 are expected to be large earthquakes in the regions denoted by the white rectangles in Figure 4 (Bilham and Hough 2006).

According to a recent paleo-seismological study, the Dauki fault, which was previously believed to be the source of the Great Indian Earthquake of 1897 by Oldham (1899), has been triggered three times in the preceding millennia.

4. Materials and methods

4.1. Database establishment

Assessing the liquefaction resistance of soils in Chittagong City, we analyzed SPT-N and V_s data collected from 48 boreholes. These boreholes were drilled to a depth of

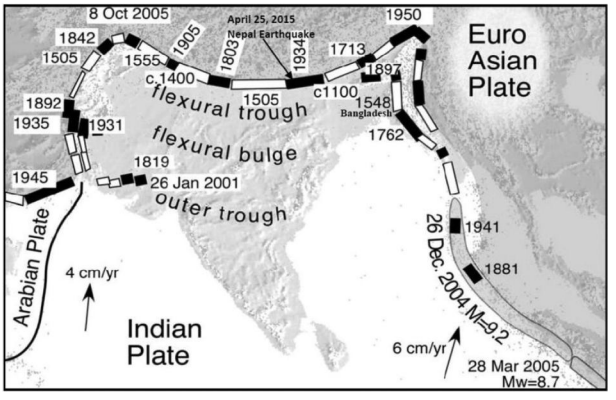

Figure 4. The continuous seismic zone delineates the boundary of the converging plate between the eurasian plate and Indian plates. Black rectangles denote high-magnitude recent earthquakes ($M > 7.5$), whereas white rectangles represent historical significant earthquakes (date indicated) and/or potential locations for significant future events ($7.5 < M < 8.5$) (Bilham and Hough 2006).

Table 2. Types of surface geological units with the corresponding quantity of Vs and SPT profiles.

Surface Geological Unit	Number of boreholes	Characterization of soil
River (H_2O)	3	HC, HS, TR
Dihing Formation Pleistocene and Pliocene (QTdi)	5	HC, HS, TR
Boka Bil Formation (Tbb)	0	HC, TR
Tipam Sandstone (Neogene) (Tt)	2	HC, HS, TR
Valley Alluvium and Colluvium (ava)	15	HC, HS, TR
Beach and Dune Sand (csd)	14	HC, HS, TR
Outside from the updated map	9	HC, HS, TR

20 meters, with samples taken every 1.5 meters. Typical borehole profiles of SPT-N can be found in the (Figure 9) and the subsurface materials' categorization is shown in the (Figure 2). We utilized the Simplified Procedure (Seed and Idriss 1971), incorporating an ANN model (Juang et al. 2000, 2002), to calculate the FS for each location. Geological units were taken into consideration while choosing the borehole sites in the city (Table 2).

To apply machine learning efficiently, it is necessary to acquire SPT and V_s data from sites where historical data on liquefaction and non-liquefaction events are available determining the points of the LSF and estimating the liquefaction indicator (LI). The LI function can reliably predict whether or not liquefaction will occur (Fahim et al. 2022). Approximately 80% of the land in this region is composed of alluvial soil, making it susceptible to liquefaction in the event of an earthquake. However, there is no recorded database of these incidents at the moment. Creating localized training datasets is difficult because of the absence of documented data. As training data is unavailable for this location, we used SPT-N data gathered by Fear and McRoberts (1993) for historical cases of both liquefaction and non-liquefaction. Idriss and Boulanger (2010) subsequently summarized this data. Andrus et al. (1999) compiled the V_s data. Datasets from Andrus et al. (1999) and Fear and McRoberts (1993) were used to train the ANN model. Andrus et al. (1999) contributed 225 instances of V_s data (containing 97 liquefaction cases) while Fear and McRoberts (1993) provided 225 instances of SPT data (including 125 liquefaction cases) from 26 earthquakes at

70 sites. This training dataset is robust and many researchers such as Fahim et al. (2022); Juang et al. (2000) used this dataset in their study and found R-values of 0.88 and 0.86 respectively.

4.2. Calculation of factor of safety (FS)

A magnitude scaling factor (MSF), Cyclic Stress Ratio (CSR), and CRR are used to determine the FS (Youd and Idriss 2001).

$$FS = \left(\frac{CRR}{CSR}\right) MSF \tag{1}$$

$$MSF = \frac{10^{2.24}}{M_w^{2.56}} \tag{2}$$

A soil layer that is $FS > 1$ is not liquefiable, but one that is $FS < 1$ is liquefiable. The amount of cycle stress (cyclic loading) generated by an earthquake is calculated employing the cyclic stress ratio, which is negatively correlated with the maximum horizontal ground acceleration ($a_{\max}$).

4.3. Calculation of CSR

$$CSR_{7.5} = 0.65\left(\frac{\sigma_v}{\sigma'_v}\right)\left(\frac{a_{\max}}{g}\right)(r_d) \tag{3}$$

Where $CSR_{7.5}$ = CSR was modified to a Mw 7.5 earthquake, considering a MSF, (a_max) = maximum ground acceleration in a horizontal direction (PGA), g = the acceleration due to gravity, σ_v = total stress, σ'_v = overall effective stress, as well r_d = coefficient of stress reduction.

The reduction coefficient can be calculated using following formula by Youd and Idriss (2001):

$$r_d = \frac{1.000 - 0.4113z^{0.5} + 0.04052z + 0.0017532z^{1.5}}{1.000 - 0.4177z^{0.5} + 0.05729z - 0.00625z^{1.5} + 0.001210z^2} \tag{4}$$

z is the depth beneath surface.

4.4. Typical calculation of CRR

Youd and Idriss (2001) calculated the typical CRR from SPT-N data using the following formula:

$$CRR = \exp\left\{\frac{(N_1)_{60cs}}{14.1} + \left(\frac{(N_1)_{60cs}}{126}\right)^2 - \left(\frac{(N_1)_{60cs}}{23.6}\right)^3 + \left(\frac{(N_1)_{60cs}}{25.4}\right)^4 - 2.8\right\} \tag{5}$$

$$(N_{1)60cs} = \alpha + \beta(N_1)_{60} \tag{6}$$

Where α and β are the coefficients and determined by following relationships:

$$\alpha = 0 \ for \ FS \leq 5\% \tag{7a}$$

$$\alpha = \exp\left[1.76 - \frac{190}{FC^2}\right] \ for \ 5\% < FS < 35\% \tag{7b}$$

$$\alpha = 5.0 \ for \ FS \geq 35\% \tag{7c}$$

$$\beta = 1.0 \ for \ FS \leq 35\% \tag{7d}$$

$$\beta = \exp\left[0.99 + \frac{FC^{1.5}}{1000}\right] for \ 5\% < FS < 35\% \tag{7e}$$

$$\beta = 1.2 \ for \ FS \leq 35\% \tag{7f}$$

The term $(N_1)_{60}$ denotes normalized SPT-N of an overburden pressure of about 100 kPa.

$$(N_1)_{60} = N_m C_N C_E C_B C_R C_s \tag{8}$$

Where N_m = SPT-N value, $C_N = N_m$ normalization factor regarding overburden stress, C_E= 60/100 = corrected hammer energy ratio, C_B = Borehole diameter adjustment, C_R = correction factor and C_s = sampler correction.

Furthermore, CRR calculated from V_s data according to Youd and Idriss (2001):

$$V_{s1} = V_s\left(\frac{P_a}{\sigma'_{v0}}\right)^{0.25} \tag{9}$$

Where V_{s1} = Overburden-stress corrected V_s, P_a = atmospheric pressure (100 kPa), σ'_{v0}=initial effective vertical stress.

$$CRR = a\left(\frac{V_{s1}}{100}\right)^2 + b\left(\frac{1}{V*_{s1} - V_{s1}} - \frac{1}{V*_{s1}}\right) \tag{10}$$

Where $V*_{s1}$= limiting upper value of V_{s1} for liquefaction occurance, a and b = curve fitting parameters whereas values are 0.022 and 2.8, respectively.

4.5. Calculation of CRR using machine learning

We will try to introduce a machine learning algorithm which is ANN. In the beginning, we developed a LI function by training neural networks model on data from real-world field cases. The resulting LI function is a predictive tool capable of

accurately distinguishing between liquefaction and non-liquefaction events (Fahim et al. 2022). Typically, the LI function (Eq.11) is a multi-dimensional and highly non-linear function. It was constructed using a three-layer neural network model:

$$LI = f_T[B_0 + \sum_{k=1}^{n}\{W_k f_T(B_{HK} + \sum_{i=0}^{m} W_{ik}P_i)\} \tag{11}$$

where B_0 represents the skew at the resultant layer when it contains only one neuron; W_k represents the weight on the link between a single output layer neuron and neuron k in the hidden layer; B_{HK} symbolizes the bias at the hidden layer's neuron k ($k = 1$, n); W_{ik} indicates the degree to which neuron k in the hidden layer is connected to the input variable i (i =1, m). Furthermore, the constructed classifier is utilized to create a searching technique that may be used to look to get points on the unidentified limit state surface. Moreover, the LSF is derived collectively from the data points and is estimated using regression analysis. Finally, to calculate the CRR, neural network models were developed on the SPT and V_s datasets.

Conceptually, the ANN model summaries potential forms that The LI function derived from the V_s and SPT data may imply, as proposed by Juang et al. (2002).

$$LI_{SPT} = f((N_1)_{60}, FCI, \sigma'_v, R_p, S_L) \tag{12}$$

$$LI_{vs} = f(V_{s1}, FCI, CSR_{7.5}) \tag{13}$$

Where, $(N_1)_{60}$ = corrected SPT-N value accounting for 100 kPa overburden and 60% hammer efficiency, V_{s1}= overburden-stress corrected V_s, FCI = fine content index, σ'_v = effective stress, R_p= pore pressure ratio, S_L= seismic loading parameter.

Here, the critical CRR, as a function of soil property indices, establishes the limit state.

$$CRR = f_T\left[B_0 + \sum_{k=1}^{n}\left\{W_k f_T\left(B_{HK} + \sum_{i=0}^{m} W_{ik}P_i\right)\right\}\right] \tag{14}$$

Conceptually, the ANN model shapes corresponding to the LSF derived from the V_s and SPT data could be as suggested by Juang et al. (2002):

$$CRR_{SPT} = f((N_1)_{60}, FCI, \sigma'_v, R_p \tag{15}$$

$$CRR_{vs} = f(V_{s1}, FCI) \tag{16}$$

The conceptual framework for this technique is displayed in (Figure 5). A point over the unknown limit state surface represents each liquefied case in the gathered database. By reducing the seismic load (route A in Figure 5), the limit state is sought after. Conversely, every non-liquefied instance within the database has symbolized as a point situated beneath the unidentified limit state surface. Presently, the seismic load (route B in Figure 5) is increased in order to seek for the limit state. Similarly, in the event that no liquefaction occurs, the seismic load can be increased (as path C in Figure 5) or the standardized soil strength parameters can be decreased (as path D in Figure 5) to produce critical CRR values for the LSF.

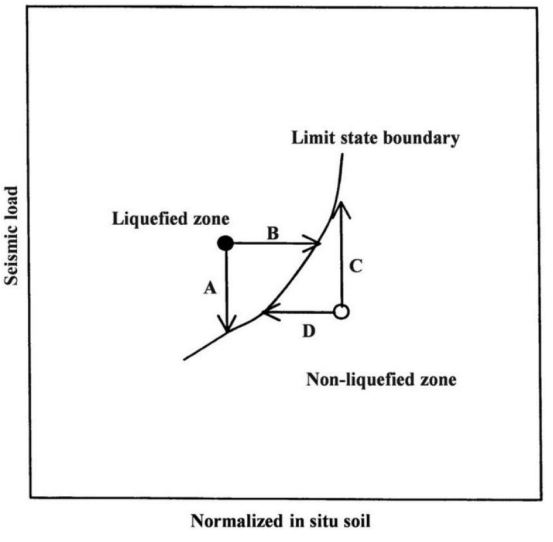

Figure 5. The search for a limit state boundary mechanism's conceptual model (Juang et al. 2000).

Table 3. Details for limit state functions (LSFs) and liquefaction indicator (LI) ANN models.

Network type	Transfer function	Training Function (both the output layer and the hidden layer)	Performance function	Adaptation learning function
Feed-forward Backpropagation	Hyperbolic Tangent Sigmoid (tansig)	Levenberg-Marquardt (TRAINLM)	Mean squared error	Gradient descent with momentum (LEARNGDM)

Table 4. The quantity of neurons and layers hidden in the limit state functions (LSFs) and liquefaction indicator (LI) ANN model.

	CRR_{SPT}	CRR_{Vs}	LI_{SPT}	LI_{Vs}
The count of layers	3	3	3	3
The number of neurons that are hidden	5	4	8	6

A multidimensional data point is produced on the limit state's surface from every search that would be successful. The boundary surface of the limit state is determined by CRR = $CRR_{7.5}$ or critical CSR, CRR in respect to soil quality indices characterizes an LSF once a sufficient number of data points have been collected.

The ANN model parameters for training, which were implemented using MATLAB's toolbox for neural networks in LI and LSFs, respectively, are displayed in Tables 3 and 4.

MATLAB provides a programming language and a realistic computational platform with several built-in algorithms. It offers a network neural toolbox with source code for all of these neural network training algorithms, like the Levenberg-Marquardt (LM) algorithm, which may be modified based on the conditions given (Fahim et al. 2022). The searching mechanism suggested is shown in (Figure 6).

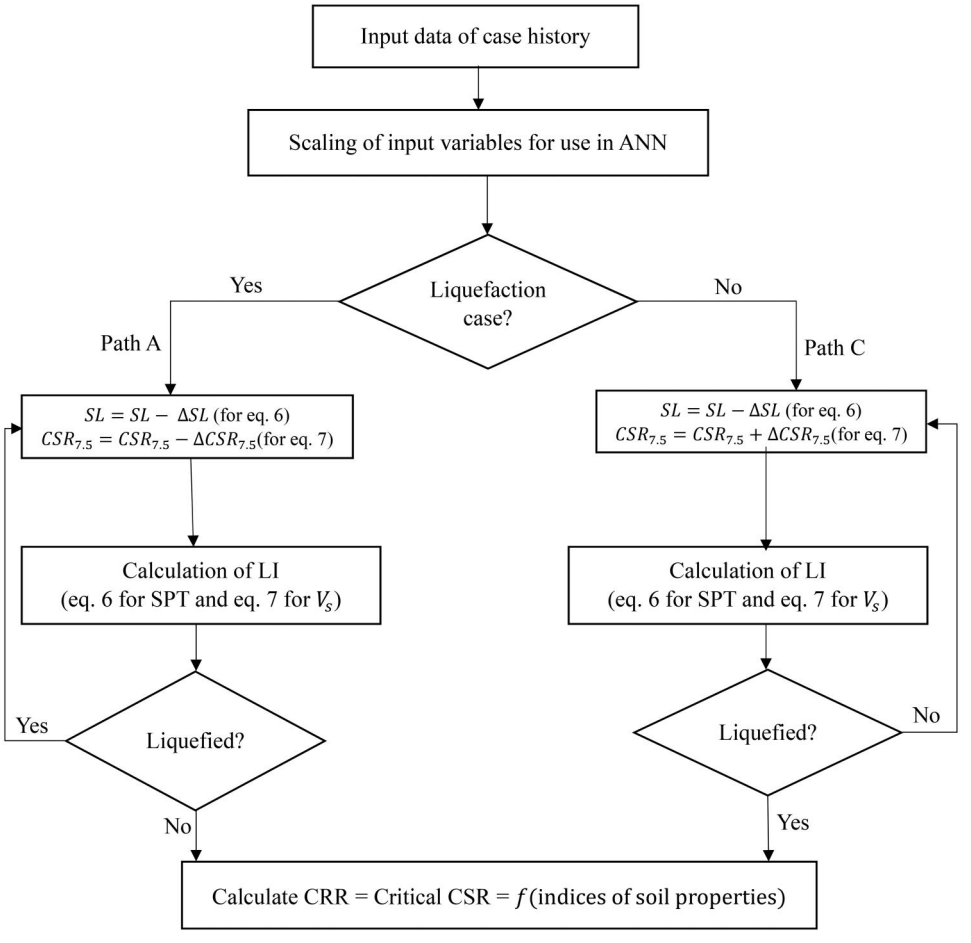

Figure 6. Searching mechanism for critical CSR or CRR (after [Juang et al. 2000]).

4.6. Calculation of LPI

Evaluation of liquefaction and its potential for destruction at each site should not solely rely on the FS. Nonetheless, the FS as well as the liquefiable layer's thickness and depth are both essential factors for liquefaction-based injury potential. The LPI is now a useful tool since it takes thickness, FS, and depth into account as inputs (Rahman et al. 2015). LPI calculates the severity of liquefaction by combining the liquefied layer's thickness and depth with their deviation from a secure FS $>$ 1.0 (Rahman and Siddiqua 2017).

$$LPI = \int_0^{20} F(z)W(z)dz \tag{17}$$

Where
$F(z) = 1 - F_z$ for $F_z < 1.0$
$F(z) = 0$ for $F_z \geq 1.0$
$W(z) = 10 - 0.5z$ for $z < 20m$

$W(z) = 0$ for $z > 20m$; where z is the distance in meters from the ground's surface.

4.7. SPT and V_s based LSF

The current study developed a performance indicator called the LI function using a data-driven methodology. This algorithm was trained on a carefully selected sample of 225 field-tested examples and was specially tailored for each set of data. Using the hold-out method, the sample was divided into two subsets, 85% for training and 15% for testing. For training SPT data, we applied indices of soil properties ($(N_1)_{60}$, FCI, σ'_v, R_p, and S_L) as input features and the output feature was CRR. Similarly for *Vs* data, in the input features, we used V_{s1}, FCI, and CSR and the target feature was CRR. The determination coefficient (R) value is one of the most reliable indicators of the effectiveness of an ANN model. For the ANN model of the LI function, the R-values for training and testing on SPT-N data were 0.886 and 0.92, respectively, while the R-values for training and testing on V_s data were 0.89. Subsequently, the searching mechanism illustrated in (Figure 6) was employed to generate locations within the boundary of the limit state, aided by the corresponding LI functions for distinct datasets. For the V_s and SPT datasets, respectively, the searching process produced a total of 236 and 143 points on the limit state surface. Following that, neural networks were trained using these data points to estimate the LSF for the corresponding datasets (Equations 15 and 16).

5. Result

The inputs (indices of soil properties) and the output (CRR) have a true but unknown functional link that is approximated by the trained neural networks. To evaluate the performance of the ANN model, we compared its predicted output values to the actual field performance data. Figures 7 and 8 illustrate this comparison for both training and testing data, using the (Equations 15 and 16) to generate data

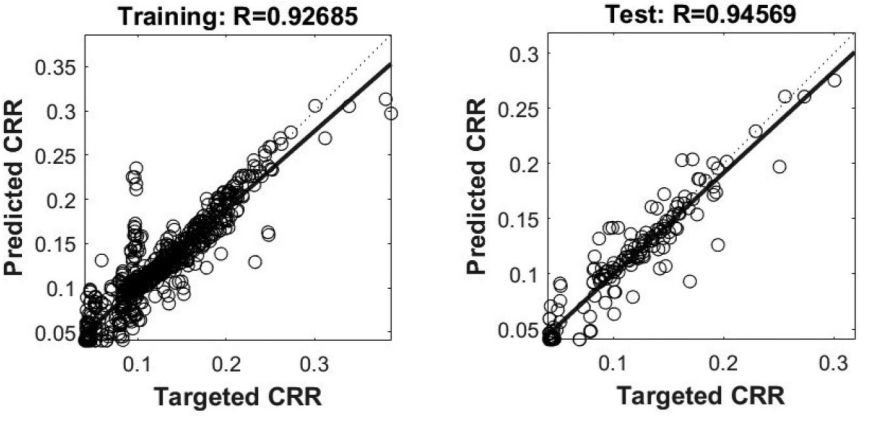

Figure 7. CRR_{SPT} model performance.

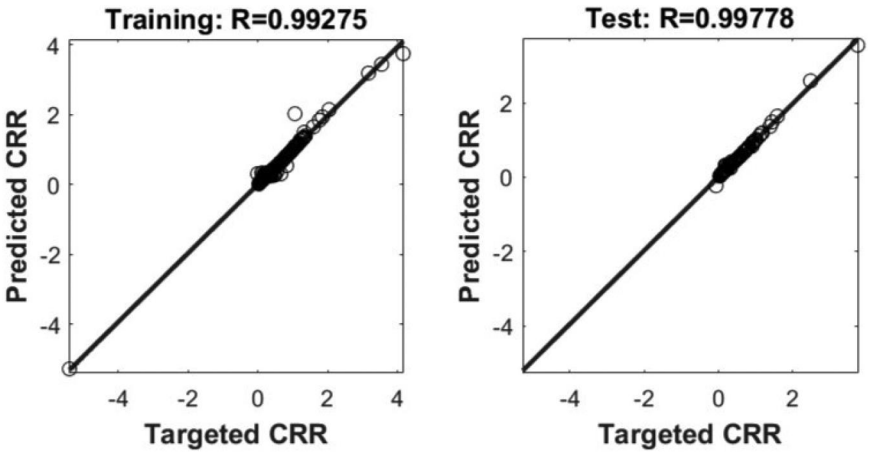

Figure 8. CRR_{Vs} model performance.

Table 5. Connection weights and biases in CRR_{SPT} (modified from Fahim et al. (2022)).

Hidden Neuron (HN) no	Weight					Bias	
	Wik				W_k	B_k	B_o
	$(N1)_{60}$ $(i=1)$	FCI $(i=2)$	σ_v' $(i=3)$	R_p $(i=4)$	Output neuron	Hidden layer	Output layer
HN 1 $(k=1)$	− 1.9681	1.2399	0.93542	− 0.71182	− 36.1196	1.8671	− 46.7613
HN 2 $(k=2)$	0.52733	0.94369	− 1.2764	1.735	20.171	− 0.53251	
HN 3 $(k=3)$	− 1.663	0.98884	1.0491	− 0.56474	82.5362	2.175	
HN 4 $(k=4)$	− 4.7013	− 2.7607	30.4863	− 44.1878	0.28948	− 33.1536	
HN 5 $(k=5)$	0.42838	0.93002	− 1.2782	1.7321	− 20.1837	− 0.60614	

Table 6. Connection weights and biases in CRR_{Vs} (modified from Fahim et al. (2022)).

Hidden neuron (HN) no	Weight		Bias		
	Wik		W_k	B_k	B_o
	V_{s1} $(i=1)$	FCI $(i=2)$	Output neuron	Hidden layer	Output layer
HN 1 $(k=1)$	1.1607	0.032301	16.9411	− 2.7486	17.0539
HN 2 $(k=2)$	− 119.0633	− 5.0242	− 21.8624	− 29.4215	
HN 3 $(k=3)$	109.4112	4.7075	16.1528	27.7892	
HN 4 $(k=4)$	106.6118	4.5549	− 38.0221	26.6818	

points along the limit state surface. These plots are based on SPT-N and V_s data. Tables 5 and 6 list the weights and biases of the connections in the trained ANN models for SPT-N and V_s data, respectively.

Normalized parameters as in (Equations 15 and 16) of each site were used to determine FS values derived from the CSR and CRR data, which were acquired through training ANN models for the LSF simulation. The FS values were computed by taking normalized parameters found in (Equations 15 and 16) of each site and computing them using the CSR and CRR values obtained from training ANN models for the LSF. According to (Eq.17), we calculated LPI values based on the FS of the SPT-N and V_s datasets. The results are presented in the Table 7.

Table 7. LPI from SPT and Vs considering a magnitude 7.5 (Mw) earthquake and PGA values of 0.15 and 0.28 g.

Borehole No.	Latitude	Longitude	GWL(m)	LPI from SPT		LPI from Vs		Surface Geological Unit Symbol
				For 0.15 g	For 0.28 g	For 0.15 g	For 0.28 g	
01	22.445417	91.816972	1.80	15.37	40.24	13.51	34.76	ava
02	22.398306	91.865306	1.80	23.67	48.40	33.00	50.74	ava
03	22.391222	91.810194	1.80	17.13	42.91	11.98	32.31	Tt
04	22.346056	91.849139	1.80	27.90	51.46	26.95	44.53	ava
05	22.365417	91.772528	1.80	18.02	40.90	13.11	34.00	csd
06	22.362056	91.761278	1.80	23.18	48.59	37.17	54.39	csd
07	22.358472	91.779861	1.80	28.80	43.11	8.06	18.14	csd
08	22.283917	91.784556	1.80	30.64	52.96	0.39	11.63	csd
09	22.236667	91.795667	1.80	28.49	51.44	9.11	24.91	csd
10	22.240250	91.815333	1.80	25.34	48.98	9.87	27.58	H_2O
11	22.424400	91.867200	1.83	33.69	53.21	17.47	37.28	ava
12	22.389700	91.874700	2.13	17.46	43.17	25.63	39.54	H_2O
13	22.378900	91.856900	1.30	25.59	56.63	33.86	51.01	ava
14	22.366111	91.849100	1.83	21.55	48.07	26.43	42.62	ava
15	22.367200	91.848889	2.44	17.10	42.72	24.45	37.34	ava
16	22.370200	91.832800	0.76	51.24	70.28	24.43	34.53	ava
17	22.371300	91.816700	1.42	18.35	42.97	22.20	33.68	QTdi
18	22.392200	91.812500	1.22	40.73	64.82	21.71	39.59	Tt
19	22.399100	91.833000	0.73	32.64	54.40	15.19	37.87	ava
20	22.337800	91.834200	2.74	9.90	40.24	14.50	38.44	ava
21	22.345300	91.797800	1.80	39.14	50.91	12.48	17.97	csd
22	22.327800	91.796100	3.60	13.19	37.05	12.85	27.30	csd
23	22.334100	91.785800	4.10	11.33	31.63	13.20	22.49	csd
24	22.313900	91.784100	2.13	38.13	54.33	10.75	27.61	csd
25	22.303300	91.775500	4.26	12.29	31.47	3.38	9.57	csd
26	22.293900	91.781100	3.90	9.55	27.60	7.23	20.21	csd
27	22.309400	91.768000	1.80	53.48	65.21	3.19	25.37	csd
28	22.365800	91.780500	3.90	20.39	25.55	0.00	0.00	csd
29	22.396222	91.757611	0.75	24.84	47.43	5.98	16.04	csd
30	22.390750	91.777778	3.50	0.77	22.23	0.00	11.98	Tbb
31	22.332806	91.770972	1.20	40.04	61.04	0.00	13.36	csd
32	22.258278	91.786222	1.20	55.03	71.45	14.09	34.06	csd
33	22.377972	91.846806	1.20	40.68	64.80	12.11	27.81	ava
34	22.351917	91.822611	3.50	10.75	32.40	6.40	27.98	ava
35	22.362944	91.842750	1.50	21.41	47.82	16.50	41.95	ava
36	22.257833	91.844750	4.20	0.00	13.27	4.33	12.01	csd
37	22.245972	91.862222	0.30	30.69	34.20	0.00	0.00	ava
38	22.226806	91.834000	0.70	28.88	58.47	29.62	41.92	csd
39	22.469972	91.803389	0.91	25.31	56.46	21.19	39.47	QTdd
40	22.439583	91.808556	0.91	26.44	53.34	0.79	26.24	QTdi
41	22.406611	91.881778	3.00	10.75	29.28	18.55	31.74	ava
42	22.397833	91.822333	0.76	25.26	55.80	20.89	38.91	QTdi
43	22.354250	91.803222	0.60	30.80	47.32	0.00	7.48	QTdi
44	22.344528	91.810250	5.50	0.17	13.82	0.00	6.45	QTdi
45	22.324333	91.809833	2.13	13.73	39.56	21.46	36.96	ava
46	22.422333	91.741556	1.80	10.50	38.71	0.00	18.37	csd
47	22.251861	91.820500	0.91	58.62	70.58	10.79	36.85	H_2O
48	22.206639	91.843444	0.91	19.88	41.96	0.00	0.22	csd

The geological unit on the surface of Chittagong City is divided into six types (Table 2). The liquefaction hazard's spatial distribution within the city is shown using LPI values formed by 48 borehole profiles and contour maps in Figures 10 and 11 for SPT and V_s respectively, with a PGA of 0.15 g and in Figures 12 and 13 for SPT and V_s correspondingly, with a PGA of 0.28 g. Inverse distance weighting (IDW) interpolation in ArcGIS is used for contour generation based on surface geologic

units and depth of soil deposits. Valley Alluvium and Beach or Dune Sand during strong ground motions, as displayed on a hazard map of the potential locations.

6. Discussion

The liquefaction hazard map provides a means of quantitatively estimating Chittagong City's susceptibility to liquefaction. To determine the spatial

Location:C.J.S high school, Kalurghat, Chittagong — G.W.L: 2.13m

Latitude:22°23'22.92" — Longitude:91°52'28.92" — Date: 07-05-08 to 08-05-08

Thickness (M)	Depth (meter)	Sample No	Lithologic Description	Bore Log	SPT Values 15cm	15cm	15cm	30cm	SPT Curve
	Extg. G.L								
3	1.5	D-1	Brownish grey, medium stiff, clayey SILT trace sand		2	3	4	7	
	3.0	D-2			2	2	3	5	
7	4.5	D-3	Grey, very soft, clayey SILT trace sand.		1	1	1	2	
	6.0	D-4			1	1	1	2	
	7.5	D-5			1	0	1	1	
	9.0	D-6			1	1	1	2	
	10.5	D-7			1	1	1	2	
3	12.0	D-8	Grey, medium stiff, clayey SILT, trace sand.		2	2	3	5	
	13.5	D-9			1	1	2	3	
5	15.0	D-10	Grey, medium dense. Medium to fine grained SAND trace silt.		4	8	8	16	
	16.5	D-11			3	6	9	15	
	18.0	D-12			6	9	14	23	
12	19.5	D-13	Bluish grey, medium stiff, CLAY, little silt.		2	3	4	7	
	21.0	D-14			2	3	3	6	
	22.5	D-15			2	3	3	6	
	24.0	D-16			2	2	3	5	
	25.5	D-17			2	3	3	6	
	27.0	D-18			2	2	3	5	
	28.5	D-19			2	2	3	5	
	30.0	D-20			2	3	4	7	

SPT Curve: 10 20 30 40 50

Figure 9. SPT's Typical profile (borehole-12).

liquefaction potential, the liquefaction FS values from SPT and V_s at 1.5 m intervals in a borehole up to a depth of twenty meters were utilized (Figure 9). To depict the LPI values of the places without a borehole, contour lines were made using similar LPI values.

There exist certain distinctions between the results generated by SPT and V_s data, as can be seen from the resulting LPI (Table 7). Based on the observed differences, it has been discovered that LPI from V_s is frequently lower than LPI derived from SPT. Other investigations have also discovered these discrepancies (Rahman and Siddiqua 2017).

These variations may result from intrinsic uncertainties in the SPT and V_s data retrieval processes. Because different SPT equipment components have varying energy efficiency, there are errors in determining V_s. These variables include the individuals doing the test, the type of casing utilized in the borehole, and the type of instrument.

In this study, two scenarios for PGA have been developed 0.15 and 0.28 g associated with an Mw magnitude of 7.5 earthquake. Figures 10 and 12 display liquefaction susceptibility maps based on SPT, while Figures 11 and 13 show maps based on V_s (for PGA of 0.15 and 0.28 g, respectively).

In the surface geological unit of Valley Alluvium and Colluvium is the part of recent deposits is made up of fine to coarse-grained sediment that has been formed by flowing water and has a high permeability. This soil is less cohesive which makes it more susceptible to liquefaction. According to Iwasaki et al. (1984) the liquefaction susceptibility in this soil ranges from high to very high with LPI values of 9.90 to 51.24 for SPT and 6.40 to 33.86 for V_s with PGA 0.15 g.

Beach and Dune sand have low cohesion due to their loose structure, making them susceptible to liquefaction. Liquefaction susceptibility ranges from high to very high with LPI values 9.55 to 55.03 for SPT and low to very high with 0.39 to 54.39 for V_s except BH 28 and BH 31 which has a PGA of 0.15 g. Although the top layer of soil in BH 28 is loose sand, there is a layer of solid rock below it at a depth of 7.5 meters. The water table is also located at a depth of 3.9 meters. These factors mean that borehole 28 is unlikely to liquefy. But the BH 31 is exceptionally indicating the LPI values of 0.

Pleistocene Dihin soil is characterized by moderately cohesive sandy loam or sandy clay loam textures, which reduces its susceptibility to liquefaction. With the exception of boreholes (17 and 42), which have a PGA of 0.15 g, the LPI values range from 0.17 to 30 for the SPT and 0 to 0.79 for V_s. LPI values from V_s seems more reliable which indicates that the soil of Dihin formation will not liquefy. According to Iwasaki et al. (1984) boreholes (40, 43, and 44) liquefaction susceptibility is very low to low. The V_s-based LPI values for both boreholes are 20.89 and 22.20, whereas the LPI values based on SPT for boreholes (17 and 42) are 18.35 and 25.26, respectively. However, tertiary sedimentary rock (TR) is discovered after 21 meters, and groundwater levels (GWL) for these boreholes are measured at 1.42 and 0.76 meters, respectively, indicating that, despite being in the Pleistocene terrace, they are likely to liquefy.

Neogene in age, Tipam sandstone is composed of finely divided, highly permeable, moderately to highly durable sand particles. Because of its lithified state and decreased porosity, compaction increases its stability and load-bearing capability and makes it resistant to liquefaction. Nevertheless, LPI values based on SPT vary from 17.13 to 40.73, while those based on V_s varies from 11.98 to 21.78, indicating that

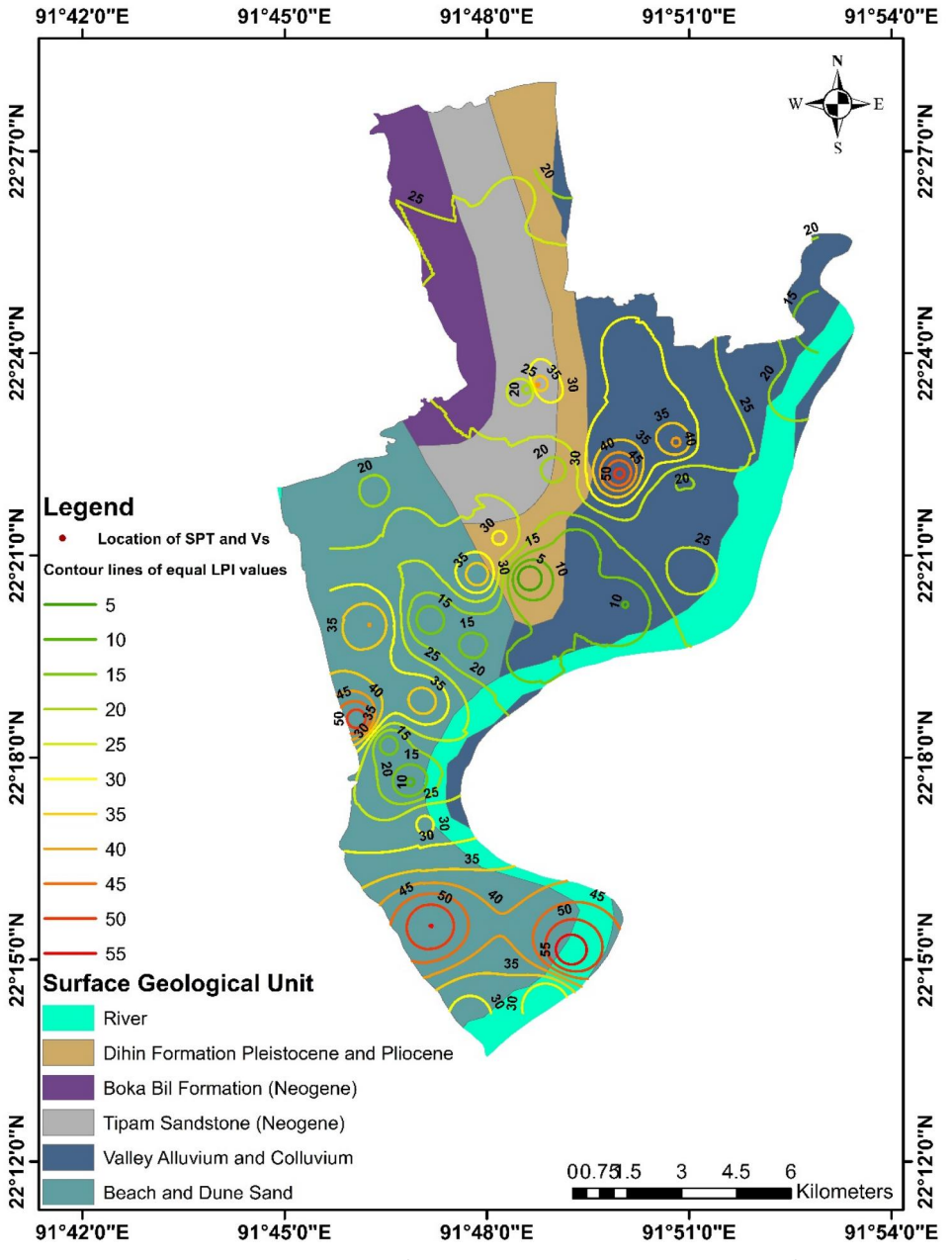

Figure 10. Based on SPT data LPI values for a Mw 7.5 earthquake with 0.15 g of PGA, Chittagong city's liquefaction hazard map.

liquefaction may be a possibility in this location. Tipam Sandstone exhibits liquefaction potential despite having a Neogene origin and being found at a depth of 21 meters with a GWL of about 1 m. Three boreholes (10, 12 and 47) are submerged within water bodies. The LPI values based on SPT differ from 17.46 to 58.62 while LPI values based on V_s differs between 9.87 and 25.63, indicating high to very high susceptibility of liquefaction in these areas.

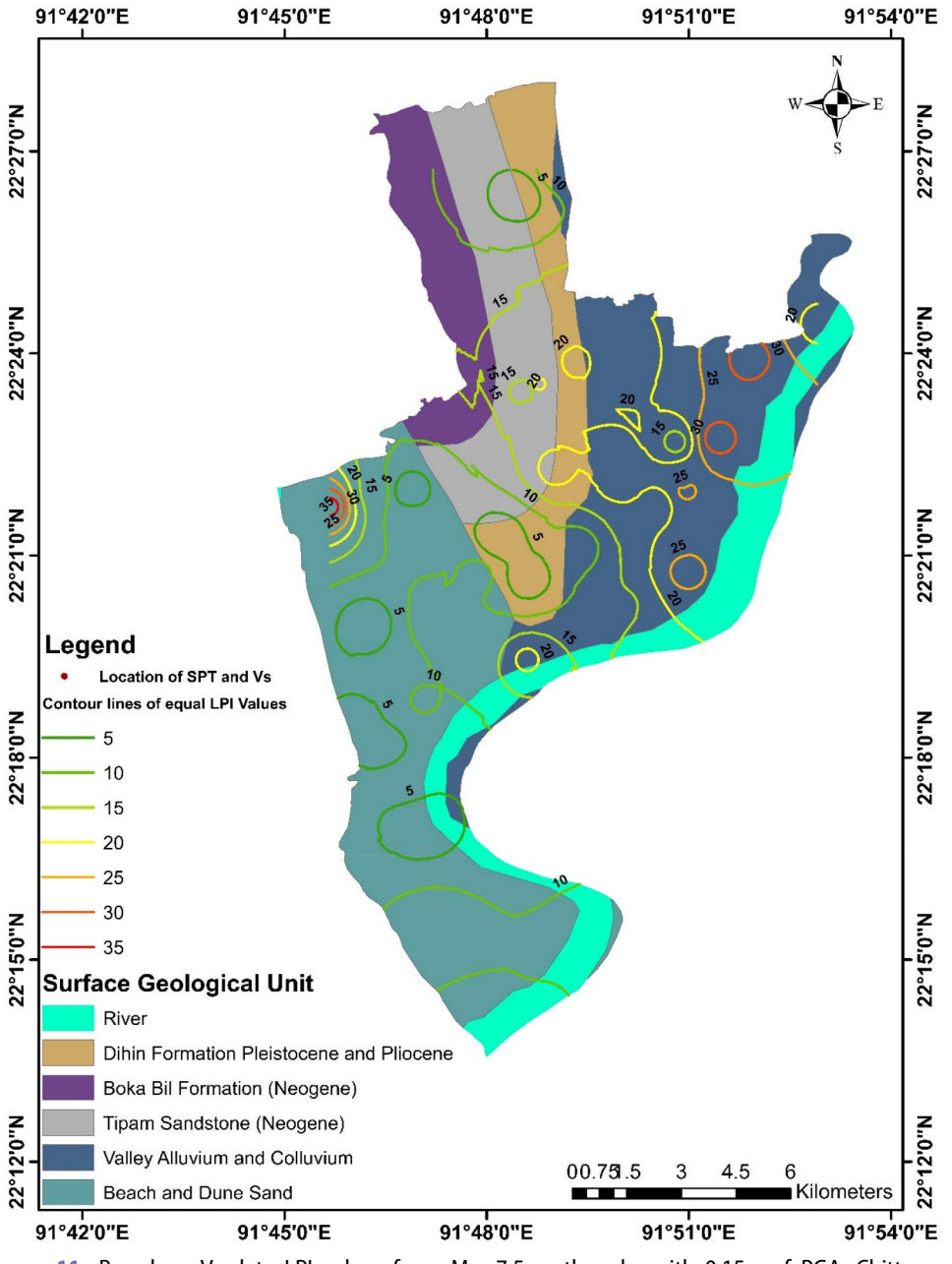

Figure 11. Based on Vs data LPI values for a Mw 7.5 earthquake with 0.15 g of PGA, Chittagong city's liquefaction hazard map.

There are nine boreholes (11, 29, 30, 36, 37, 38, 39, 46, and 48) that are not on the most recent Chittagong city corporation map.

For the scenario of PGA 0.28 g, Valley Alluvium, and Colluvium the liquefaction susceptibility in this soil is very high with LPI values 29.28 to 70.28 for SPT and 27.81 to 51.01 for V_s. Liquefaction susceptibility is high to very high in Beach and Dune Sand with LPI values 9.55 to 55.03 for SPT and 9.57 to 54.39 for V_s except

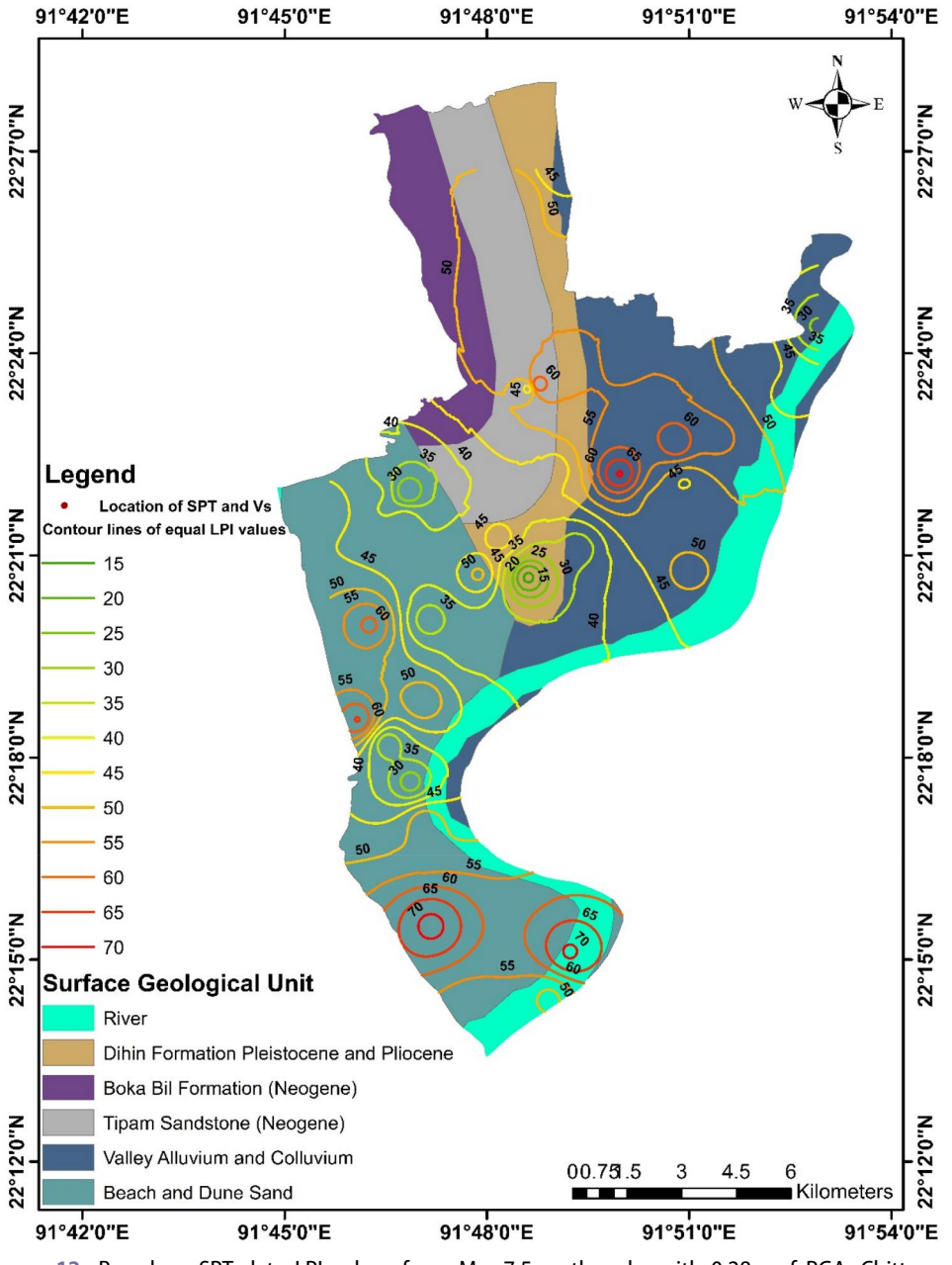

Figure 12. Based on SPT data LPI values for a Mw 7.5 earthquake with 0.28 g of PGA, Chittagong city's liquefaction hazard map.

borehole 28. The LPI value for borehole 28 is 25.5, 0 from the SPT and V_s, respectively. At 7.5 meters, we have a layer of solid rock and the water table is at 3.9 meters below ground level. As such, the LPI based on V_s appears to be more viable for this borehole suggesting that this region is not prone to liquefaction. The susceptibility of Dihin formation (Pleistocene) to liquefaction is categorized as extremely high to high with LPI values ranging from 13.52 to 55.80 and 6.45 to 38.91 for SPT and V_s,

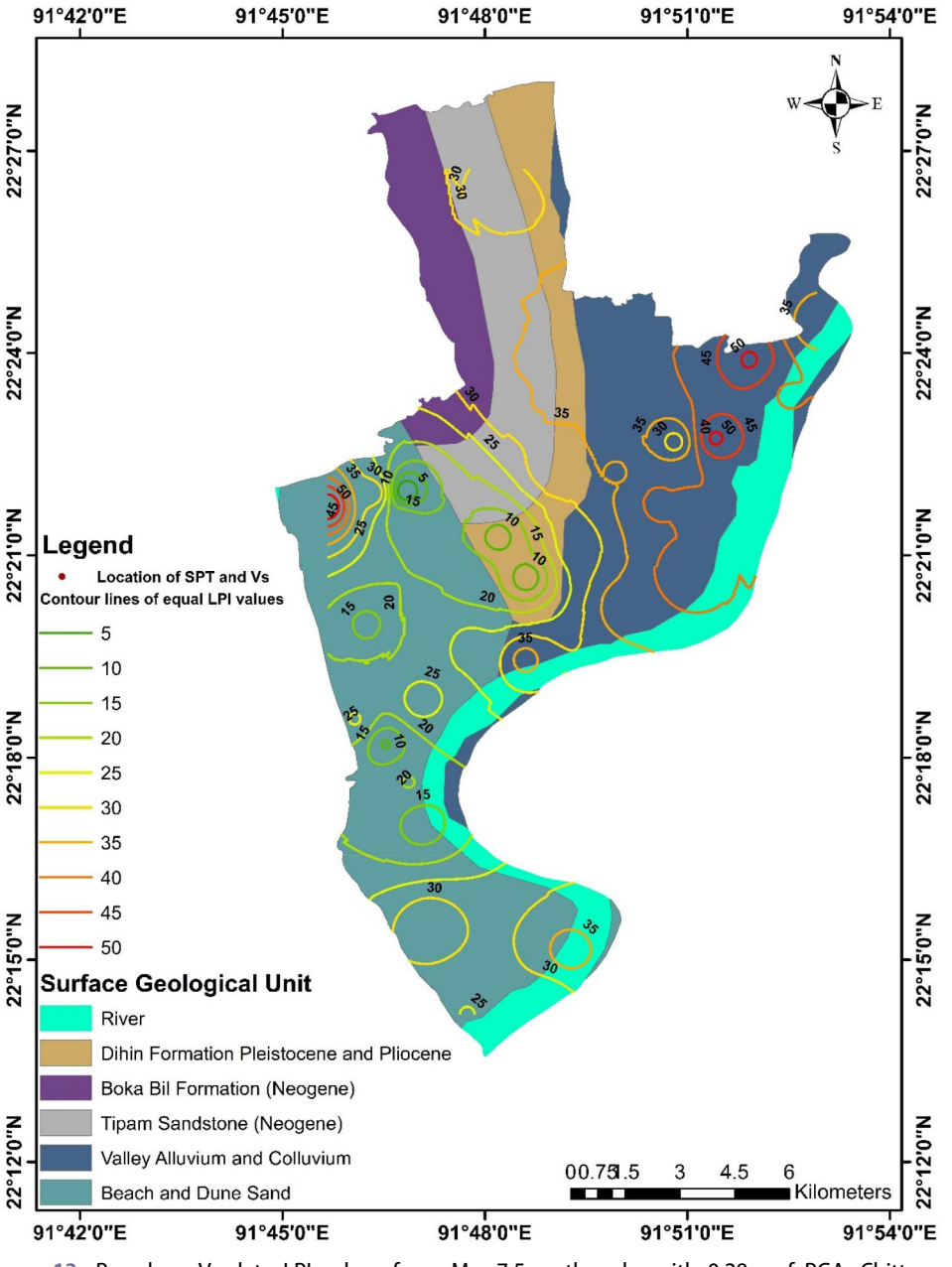

Figure 13. Based on Vs data LPI values for a Mw 7.5 earthquake with 0.28 g of PGA, Chittagong city's liquefaction hazard map.

correspondingly. Tipam sandstone in the Neogene epoch's susceptibility level of liquefaction is very high with LPI values ranging from 42.91 to 64.82 and 32.31 to 39.59 for SPT and V_s, respectively. Even though Tipam Sandstone is Neogene in origin and is located at a depth of 21 meters with a GWL of roughly one meter, it shows liquefaction potential. Three boreholes are submerged within the river, in this

Table 8. Liquefaction hazard classification based on LPI values (according to Iwasaki et al. (1984)).

Liquefaction classes	LPI values
Very Low	LPI = 0
Low	0 < LPI = <5
High	5 < LPI = < 15
Very High	LPI > 15

Table 9. Comparison between Rahman and Siddiqua (2017) and the present study.

	Current Study			Rahman and Siddiqua (2017)		
		LPI values for 0.15g			LPI values for 0.15g	
Surface Geological Unit	Borehole No	SPT	Vs	Borehole No	SPT	Vs
Valley Alluvium and Colluvium	2	23.67	33	1	14.7	22.6
Tipam Sandstone (Neogene)	3	17.13	11.98	2	0	0
Valley Alluvium and Colluvium	34	10.75	6.4	3	13.1	7.8
Beach and Dune Sand	5	18.02	13.11	4	11.2	10.7
Beach and Dune Sand	7	28.8	8.06	5	10.5	14.9
Beach and Dune Sand	9	28.49	9.11	6	17.3	13.7
	Mean	21.14	13.61		11.13	11.62
	Minimum	10.75	6.4		0	0
	Maximum	28.8	33		17.3	22.6

area, the LPI values varied from 43.17 to 70.58 and 27.58 to 39.54 in that order, which recommends that this area is highly prone to liquefaction (Table 8).

Rahman and Siddiqua (2017) used limited V_s and SPT data to examine the liquefaction potential of the cities of Sylhet, Chittagong, and Dhaka in Bangladesh. They utilized six PS logging borehole datasets for Chittagong city and shallow seismic data from CDMP (2009) in the present study. The boreholes of this study (2, 3, 34, 5, 7, and 9), correspond to PS logging boreholes (1 to 6) in the study of Rahman and Siddiqua (2017). Since PS logging can directly detect and monitor micro seismic events associated with soil displacement and deformation which are the indicators of probable liquefaction. Consequently, it is frequently more accurate than shallow seismic approaches for assessing liquefaction. The comparison of LPI values and statistical components between the present study and Rahman and Siddiqua (2017) is shown in Table 9. Limited publications exist on paleo-seismological studies in Bangladesh, particularly around Chittagong City (Morino et al. 2014). This is challenging due to the rapidly changing sedimentary basin (Bengal Basin) over the past century (Rahman and Siddiqua 2017). Researchers use various threshold values of the LPI from existing literature to validate liquefaction hazard results (Rahman and Siddiqua 2017). Since actual field validation cannot be achieved, in this study, we calculated LPI using both a simplified procedure and a machine learning algorithm that increases the reliability of LPI values.

Historical earthquake records in Bangladesh show liquefaction occurrences in the sandy and silty alluvium of Holocene floodplains during earthquakes in Bengal in 1885 (M_w 6.87), Great Assam in 1897 (M_w 8.03), and Srimangal in 1918 (M_w 7.2) (Fahim et al. 2022; Morino et al. 2014). The current study's findings imply that, in the event of a M_w 7.5 earthquake with 0.15 g of PGA, extreme liquefaction might

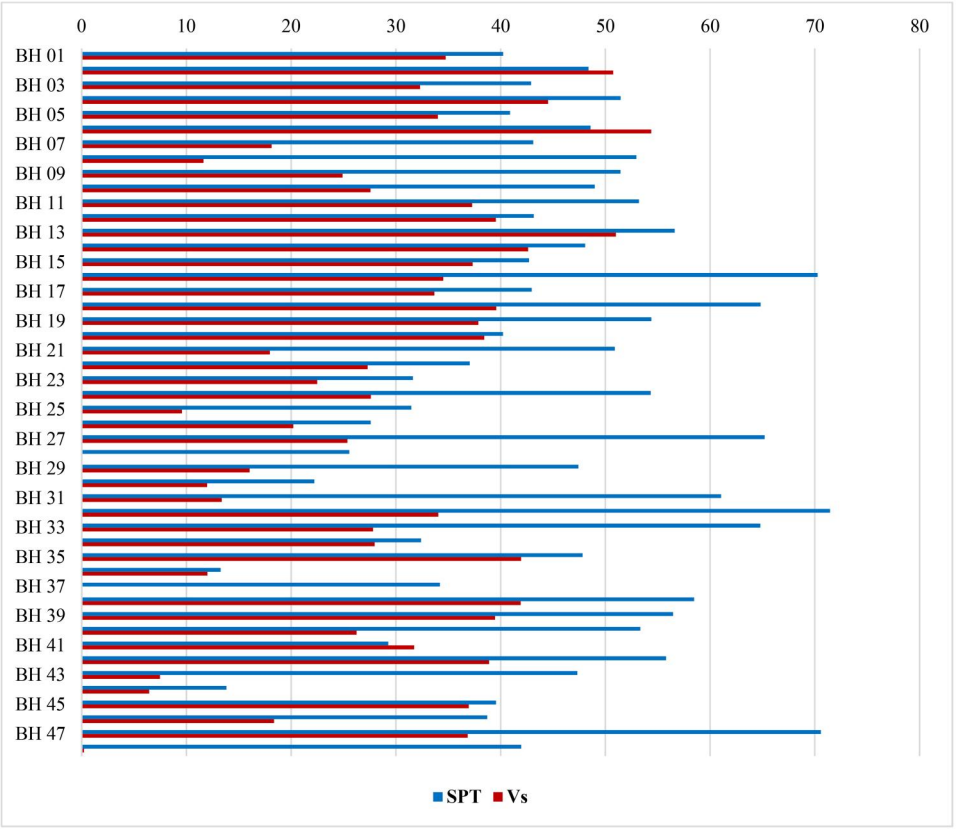

Figure 14. A comparison between the SPT and Vs method LPI values with a PGA of 0.28 g.

happen in the Valley Alluvium and Beach or Dune Sand, and Dihin and Tipam will not liquefy in Figures 10 and 11. The current study's findings also imply that, in the event of a M_w 7.5 earthquake with 0.28 g of PGA, Valley alluvium, and Beach or Dune sand are extremely susceptible, Dihin formation is mild, Tipam Sandstone is variable, and submerged places are susceptible in Figures 12 and 13.

From the Figure 14, it has been observed that in most boreholes, the LPI value calculated using SPT exceeds that calculated using V_s. SPT provides data on soil density and resistance by measuring the soil's resistance to penetration with a drill and hammer. In order to determine the stiffness and soil density, V_s evaluates how quickly shear waves pass through the material. The differences in the parameters observed, the depiction of soil behavior, site-specific factors, and the modeling assumptions connected with each test method are the causes of the discrepancy in LPI between SPT and V_s.

For evaluating the performance of the ANN-based approach, a comparison against the traditional approach of calculating LPI can be found in Figure 15. The results from the ANN model indicated a good correlation to the results of the traditional method depicted by R-value of 0.78 as shown in Figure 15. This suggests a reliable level of agreement between the two approaches. While some scatter is observed, the

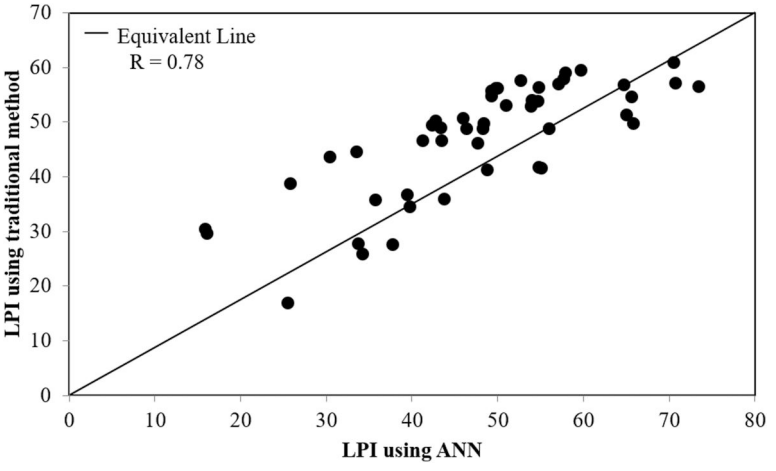

Figure 15. Comparison between ANN-based approach and traditional approach.

ANN-based predictions align well with the equivalent line which demonstrates its potential as a viable alternative to traditional methods.

The study has several limitations that impact its accuracy and precision. Firstly, groundwater level (GWL) data was missing for boreholes 1 to 10 and 29 to 38, necessitating the use of a mean GWL of 1.80 meters for these boreholes based on Fahim et al. (2022, 2023). Additionally, percentages of fines for boreholes 1 to 10 and 29 to 38 were unavailable, requiring estimations based on expert judgments. Furthermore, unit weights were not provided for these boreholes and were instead computed from SPT data according to M. Rahman (2019). Moreover, nine boreholes (11, 29, 30, 36, 37, 38, 39, 46, and 48) were not depicted on the most recent Chittagong City Corporation map, leading to their exclusion from liquefaction susceptibility mapping. These limitations highlight the importance of accurate and comprehensive data for reliable liquefaction hazard analysis. The uncertainties associated with the estimation of LPI can be declined by using more SPT-N and V_s data and more precise data on GWL, percentage of fines, unit weight and ground motion parameters.

7. Conclusion

ANN model uses sufficient real-world performance cases, it yields more reliable and realistic results while estimating the CRR using the V_s and SPT data. That is the reason ANN was taken into account for calculating CRR in this study. Using the CRR, the FS is computed using PGA values of 0.15 and 0.28 g and an earthquake of magnitude (M_w 7.5). Subsequently, the liquefiable layers' thickness and the FS of liquefaction have been used to calculate the LPI. The current study reveals that:

1. The majority of boreholes, the LPI value based on SPT is greater than V_s.
2. Extreme liquefaction might happen in the Valley Alluvium and Beach or Dune Sand which cover the most of the area of Chittagong City.

3. The LPI values vary between 9.55 to 55.03 for SPT and 0 to 37.17 for V_s, with a PGA of 0.15 g. For a PGA of 0.28 g, LPI ranges from 25.55 to 71.45 for SPT and 9.55 to 54.39 for V_s, except for borehole-28.

As a result, liquefaction hazard analysis is extremely important for this city for the evaluation of seismic hazards and the seismic structure of buildings. The Chittagong City liquefaction hazard map can be used in urban planning, disaster preparedness, and risk awareness by identifying areas prone to liquefaction during earthquakes. It supports resilience building, research, and decision-making to minimize earthquake impacts and foster sustainable growth in Chittagong City.

Acknowledgements

The authors thank the Comprehensive Disaster Management Programme (CDMP), Bangladesh, for providing all the required data used in this study. They also thank to the Department of Disaster Science and Climate Resilience (DSCR), University of Dhaka, Bangladesh for research facilities and enabling to conduct this research. This work was supported by Centre for Urban Resilience Studies, University of Dhaka.

Disclosure statement

No potential conflict of interest was reported by the author(s).

Consent for publication

All the authors consented to publish the paper.

Code availability

The codes used for data processing can be provided at the request of the corresponding author.

References

Andrus RD, Stokoe K, Chung R, Juang C. 1999. *Draft guidelines for evaluating liquefaction resistance using shear wave velocity measurements and simplified procedures.*

Andrus RD, Stokoe KH. 2000. Liquefaction resistance of soils from shear-wave velocity. J Geotech Geoenviron Eng. 126(11):1015–1025. doi: 10.1061/(ASCE)1090-0241(2000)126:11(1015).

Bilham R, Hough S. 2006. Future earthquakes on the Indian subcontinent: inevitable hazard, preventable risk. South Asian J. 12(April–June):1–9. http://cires1.colorado.edu/~bilham/SouthAsianJourn2006.pdf.

Bilham R. 2009. The seismic future of cities. Bull Earthquake Eng. 7(4):839–887. doi: 10.1007/s10518-009-9147-0.

Bürgi P, Hubbard J, Akhter SH, Peterson DE. 2021. Geometry of the Décollement below eastern Bangladesh and implications for seismic hazard. JGR Solid Earth. 126(8) doi: 10.1029/2020JB021519.

Fahim AKF, Kamal ASMM, Shahid S. 2023. Spatiotemporal change in groundwater sustainability of Bangladesh and its major causes. Stoch Environ Res Risk Assess. 37(2):665–680. 10.1007/s00477-022-02294-z.

Fahim AKF, Rahman MZ, Hossain MS, Kamal ASMM. 2022. Liquefaction resistance evaluation of soils using artificial neural network for Dhaka City, Bangladesh. Nat Hazards. 113(2):933–963. doi: 10.1007/s11069-022-05331-w.

Fear CE, McRoberts EC. 1993. Report on liquefaction potential and catalogue of case records.

Hossain MS, Kamal ASMM, Rahman MZ, Farazi AH, Mondal DR, Mahmud T, Ferdous N. 2020. Assessment of soil liquefaction potential: a case study for Moulvibazar town, Sylhet, Bangladesh. SN Appl Sci. 2(4):1–12. doi: 10.1007/s42452-020-2582-x.

Idriss IM, Boulanger RW. 2010. SPT- based liquefaction triggerering procedures BASED.

Iwasaki T, Arakawa T, Tokida KI. 1984. Simplified procedures for assessing soil liquefaction during earthquakes. Int J Soil Dyn Earthquake Eng. 3(1):49–58. doi: 10.1016/0261-7277(84)90027-5.

Juang CH, Chen CJ, Jiang T, Andrus RD. 2000. Risk-based liquefaction potential evaluation using standard penetration tests. Can Geotech J. 37(6):1195–1208. doi: 10.1139/t00-064.

Juang CH, Jiang T, Andrus RD. 2002. Assessing probability-based methods for liquefaction potential evaluation. J Geotech Geoenviron Eng. 128(7):580–589. doi: 10.1061/(ASCE)1090-0241(2002)128:7(580).

Juang CH, Yuan H, Lee D-H, Lin P-S. 2003. Simplified cone penetration test-based method for evaluating liquefaction resistance of soils. J Geotech Geoenviron Eng. 129(1):66–80. doi: 10.1061/(ASCE)1090-0241(2003)129:1(66).

Ku C-S, Lee D-H, Wu J-H. 2004. Evaluation of soil liquefaction in the Chi-Chi, Taiwan earthquake using CPT. Soil Dyn Earthquake Eng. 24(9-10):659–673. doi: 10.1016/j.soildyn.2004.06.009.

Marcuson. 1979. Definition of terms related to liquefaction. Int J Rock Mech Min Sci Geomech Abstr. 16(2):21. doi: 10.1016/0148-9062(79)91458-X.

Morino M, Monsur MH, Kamal ASMM, Akhter SH, Rahman MZ, Ali RME, Talukder A, Khan MMH. 2014. Examples of paleo-liquefaction in Bangladesh. J Geol Soc Japan. 120(9): VII–VIII. doi: 10.5575/geosoc.2014.0032.

Muduli PK, Das SK, Bhattacharya S. 2014. CPT-based probabilistic evaluation of seismic soil liquefaction potential using multi-gene genetic programming. Georisk: Assess Manag Risk Eng Syst Geohazards. 8(1):14–28. doi: 10.1080/17499518.2013.845720.

Muduli PK, Das SK. 2013. SPT-based probabilistic method for evaluation of liquefaction potential of soil using multi-gene genetic programming. Int J Geotech Earthquake Eng. 4(1): 42–60. doi: 10.4018/jgee.2013010103.

Muduli PK, Das SK. 2014a. CPT-based seismic liquefaction potential evaluation using multi-gene genetic programming approach. Indian Geotech J. 44(1):86–93. doi: 10.1007/s40098-013-0048-4.

Muduli PK, Das SK. 2014b. Evaluation of liquefaction potential of soil based on standard penetration test using multi-gene genetic programming model. Acta Geophys. 62(3):529–543. doi: 10.2478/s11600-013-0181-6.

Muduli PK, Das SK. 2015a. Evaluation of liquefaction potential of soil based on shear wave velocity using multi-gene genetic programming. In: Gandomi A, Alavi A, Ryan C, editors. Handbook of genetic programming applications. Cham: Springer. doi: 10.1007/978-3-319-20883-1_12.

Muduli PK, Das SK. 2015b. First-order reliability method for probabilistic evaluation of liquefaction potential of soil using genetic programming. Int J Geomech. 15(3):1–16. doi: 10.1061/(asce)gm.1943-5622.0000377.

Muduli PK, Das SK. 2015c. Model uncertainty of SPT-based method for evaluation of seismic soil liquefaction potential using multi-gene genetic programming. Soils Found. 55(2):258–275. doi: 10.1016/j.sandf.2015.02.003.

Oldham RD. 1899. Report on the Great Earthquake of 12th June, 1897.

Rahman M. 2019. Foundation design using standard penetration test (SPT) N-value. Researchgate. 5(June):1–39. doi: 10.13140/RG.2.2.23159.73123.

Rahman MZ, Siddiqua S, Kamal ASMM. 2015. Liquefaction hazard mapping by liquefaction potential index for Dhaka City, Bangladesh. Eng Geol. 188:137–147. doi: 10.1016/j.enggeo.2015.01.012.

Rahman MZ, Siddiqua S, Kamal ASMM. 2016. Shear wave velocity estimation of the near-surface materials of Chittagong City, Bangladesh for seismic site characterization. J Appl Geophys. 134:210–225. doi: 10.1016/j.jappgeo.2016.09.006.

Rahman MZ, Siddiqua S, Kamal ASMM. 2020. Seismic source modeling and probabilistic seismic hazard analysis for Bangladesh. Nat Hazards. 103(2):2489–2532. doi: 10.1007/s11069-020-04094-6.

Rahman MZ, Siddiqua S. 2017. Evaluation of liquefaction-resistance of soils using standard penetration test, cone penetration test, and shear-wave velocity data for Dhaka, Chittagong, and Sylhet cities in Bangladesh. Environ Earth Sci. 76:207 doi: 10.1007/s12665-017-6533-9.

Rahman Z, Siddiqua S. 2016. Liquefaction resistance evaluation of soils using standard penetration test blow count and shear wave velocity valorization of pre-consumer apparel waste in road construction view project. November. https://www.researchgate.net/publication/309592537.

Robertson PK, Woeller DJ, Finn WDL. 1992. Cyclic large strain and induced pore pressuremodels for saturated clean sands. Can Geotech J. 29(4):686–695. doi: 10.1139/t92-075.

Robertson PK, Wride CE. 1998. Evaluating cyclic liquefaction potential using the cone penetration test. Can Geotech J. 35(3):442–459. doi: 10.1139/t98-017.

Sassa S, Takagawa T. 2019. Liquefied gravity flow-induced tsunami: first evidence and comparison from the 2018 Indonesia Sulawesi earthquake and tsunami disasters. Landslides. 16(1):195–200. doi: 10.1007/s10346-018-1114-x.

Seed HB, Idriss IM, Arango I. 1983. Evaluation of liquefaction potential using field performance data. J Geotech Eng. 109(3):458–482. http://cedb.asce.org/cgi/wwwdisplay.cgi?8300283. doi: 10.1061/(ASCE)0733-9410(1983)109:3(458).

Seed HB, Idriss IM. 1967. Analysis of soil liquefaction: Niigata earthquake. J Soil Mech Found Div. 93(3):83–108. doi: 10.1061/JSFEAQ.0000981.

Seed HB, Idriss IM. 1971. Simplified procedure for evaluating soil liquefaction potential. J Soil Mech Found Div. 97(9):1249–1273. doi: 10.1061/JSFEAQ.0001662.

Shahin MA, Jaksa MB, Maier HR. 2001. Artificial neural network applications in geotechnical engineering. Aust Geomech J. 36(1):49–62.

Xue X, Liu E. 2017. Seismic liquefaction potential assessed by neural networks. Environ Earth Sci. 76(5):1–15. doi: 10.1007/s12665-017-6523-y.

Youd TL, Idriss IM. 2001. Liquefaction resistance of soils: summary report from the 1996 NCEER and 1998 NCEER/NSF workshops on evaluation of liquefaction resistance of soils. J Geotech Geoenviron Eng. 127(4):297–313. doi: 10.1061/(ASCE)1090-0241(2001)127:4(297).